The relationship between upwelling underwater polarization and attenuation/absorption ratio

Amir Ibrahim, Alexander Gilerson, Tristan Harmel, Alberto Tonizzo, Jacek Chowdhary, Samir Ahmed

The relationship between upwelling underwater polarization and attenuation/absorption ratio

Amir Ibrahim,[1] Alexander Gilerson,[1,*] Tristan Harmel,[2] Alberto Tonizzo,[1] Jacek Chowdhary,[3] and Samir Ahmed[1]

[1]*Optical Remote Sensing Laboratory, The City College of the City University of New York, New York, New York 10031, USA*

[2]*Laboratoire d'Océanographie de Villefranche, Villefranche-sur-Mer, France*

[3]*Department of Applied Physics and Applied Mathematics, Columbia University, New York, New York 10025, USA*

[*]*gilerson@ccny.cuny.edu*

Abstract: The attenuation coefficient of the water body is not directly retrievable from measurements of unpolarized water-leaving radiance. Based on extensive radiative transfer simulations using the vector radiative transfer code RayXP, it is demonstrated that the underwater degree of linear polarization (DoLP) is closely related to the attenuation-to-absorption ratio (c/a) of the water body, a finding that enables retrieval of the attenuation coefficient from measurements of the Stokes components of the upwelling underwater polarized light field. The relationship between DoLP and the c/a ratio is investigated for the upwelling polarized light field for a complete set of viewing geometries, at several wavelengths in the visible part of the spectrum; for varying compositions of the aquatic environment, whose constituents include phytoplankton, non-algal particles, and color dissolved organic matter (CDOM); and for varying microphysical properties such as the refractive index and the slope of the Junge-type particle size distribution (PSD). Consequently, this study reveals the possibility for retrieval of additional inherent optical properties (IOPs) from air- or space-borne DoLP measurements of the water-leaving radiation.

OCIS codes: (010.4450) Oceanic optics; (010.0280) Remote sensing and sensors; (260.5430) Polarization; (010.5620) Radiative transfer.

References and links

1. Y. Liu and K. Voss, "Polarized radiance distribution measurement of skylight. II. Experiment and data," Appl. Opt. **36**(33), 8753–8764 (1997).
2. F. Waquet, B. Cairns, K. Knobelspiesse, J. Chowdhary, L. D. Travis, B. Schmid, and M. I. Mishchenko, "Polarimetric remote sensing of aerosols over land," J. Geophys. Res-Atmos. **114**(D1), D01206 (2009).
3. M. Chami, R. Santer, and E. Dilligeard, "Radiative transfer model for the computation of radiance and polarization in an ocean-atmosphere system: polarization properties of suspended matter for remote sensing," Appl. Opt. **40**(15), 2398–2416 (2001).
4. A. Tonizzo, A. Gilerson, T. Harmel, A. Ibrahim, J. Chowdhary, B. Gross, F. Moshary, and S. Ahmed, "Estimating particle composition and size distribution from polarized water-leaving radiance," Appl. Opt. **50**(25), 5047–5058 (2011).
5. H. Loisel, L. Duforet, D. Dessailly, M. Chami, and P. Dubuisson, "Investigation of the variations in the water leaving polarized reflectance from the POLDER satellite data over two biogeochemical contrasted oceanic areas," Opt. Express **16**(17), 12905–12918 (2008).
6. P. Bhandari, K. J. Voss, L. Logan, and M. Twardowski, "The variation of the polarized downwelling radiance distribution with depth in the coastal and clear ocean," J. Geophys. Res-Oceans **116**, C00H10 (2011).
7. T. Harmel and M. Chami, "Influence of polarimetric satellite data measured in the visible region on aerosol detection and on the performance of atmospheric correction procedure over open ocean waters," Opt. Express **19**(21), 20960–20983 (2011).
8. J. Chowdhary, B. Cairns, and L. D. Travis, "Contribution of water-leaving radiances to multiangle, multispectral polarimetric observations over the open ocean: bio-optical model results for case 1 waters," Appl. Opt. **45**(22), 5542–5567 (2006).
9. J. Chowdhary, B. Cairns, F. Waquet, K. Knobelspiesse, M. Ottaviani, J. Redemann, L. Travis, and M. Mishchenko, "Sensitivity of multiangle, multispectral polarimetric remote sensing over open oceans to water-

#174765 - $15.00 USD Received 21 Aug 2012; revised 16 Oct 2012; accepted 23 Oct 2012; published 29 Oct 2012

leaving radiance: analyses of RSP data acquired during the MILAGRO campaign," Remote Sens. Environ. **118**, 284–308 (2012).
10. J. E. Hansen and L. D. Travis, "Light scattering in planetary atmospheres," Space Sci. Rev. **16**(4), 527–610 (1974).
11. A. Tonizzo, J. Zhou, A. Gilerson, M. S. Twardowski, D. J. Gray, R. A. Arnone, B. M. Gross, F. Moshary, and S. A. Ahmed, "Polarized light in coastal waters: hyperspectral and multiangular analysis," Opt. Express **17**(7), 5666–5683 (2009).
12. K. J. Voss and E. S. Fry, "Measurement of the Mueller matrix for ocean water," Appl. Opt. **23**(23), 4427–4439 (1984).
13. T. Harmel and M. Chami, "Invariance of polarized reflectance measured at the top of atmosphere by PARASOL satellite instrument in the visible range with marine constituents in open ocean waters," Opt. Express **16**(9), 6064–6080 (2008).
14. D. Stramski, A. Bricaud, and A. Morel, "Modeling the inherent optical properties of the ocean based on the detailed composition of the planktonic community," Appl. Opt. **40**(18), 2929–2945 (2001).
15. M. Babin, D. Stramski, G. M. Ferrari, H. Claustre, A. Bricaud, G. Obolensky, and N. Hoepffner, "Variations in the light absorption coefficients of phytoplankton, nonalgal particles, and dissolved organic matter in coastal waters around Europe," J. Geophys. Res-Oceans **108**(C7), 3211 (2003).
16. M. Babin, A. Morel, V. Fournier-Sicre, F. Fell, and D. Stramski, "Light scattering properties of marine particles in coastal and open ocean waters as related to the particle mass concentration," Limnol. Oceanogr. **48**(2), 843–859 (2003).
17. A. Ivanoff, N. Jerlov, and T. H. Waterman, "A Comparative study of irradiance, beam transmittance and scattering in the sea near Bermuda," Limnol. Oceanogr. **6**(2), 129–148 (1961).
18. M. Chami and D. McKee, "Determination of biogeochemical properties of marine particles using above water measurements of the degree of polarization at the Brewster angle," Opt. Express **15**(15), 9494–9509 (2007).
19. M. Chami, "Importance of the polarization in the retrieval of oceanic constituents from the remote sensing reflectance," J. Geophys. Res-Oceans **112**(C5), C05026 (2007).
20. J. K. Lotsberg and J. J. Stamnes, "Impact of particulate oceanic composition on the radiance and polarization of underwater and backscattered light," Opt. Express **18**(10), 10432–10445 (2010).
21. B. Fougnie, G. Bracco, B. Lafrance, C. Ruffel, O. Hagolle, and C. Tinel, "PARASOL in-flight calibration and performance," Appl. Opt. **46**(22), 5435–5451 (2007).
22. http://www.eumetsat.int/groups/pps/documents/document/pdf_peps_mrd.pdf
23. Y. You, A. Tonizzo, A. A. Gilerson, M. E. Cummings, P. Brady, J. M. Sullivan, M. S. Twardowski, H. M. Dierssen, S. A. Ahmed, and G. W. Kattawar, "Measurements and simulations of polarization states of underwater light in clear oceanic waters," Appl. Opt. **50**(24), 4873–4893 (2011).
24. Y. You, G. W. Kattawar, K. J. Voss, P. Bhandari, J. W. Wei, M. Lewis, C. J. Zappa, and H. Schultz, "Polarized light field under dynamic ocean surfaces: numerical modeling compared with measurements," J. Geophys. Res-Oceans **116**, C00H05 (2011).
25. J. T. Adams, E. Aas, N. K. Højerslev, and B. Lundgren, "Comparison of radiance and polarization values observed in the Mediterranean sea and simulated in a Monte Carlo model," Appl. Opt. **41**(15), 2724–2733 (2002).
26. V. A. Timofeyeva, "Degree of polarization of light in turbid media," Izvestiya Akademii Nauk Sssr Fizika Atmosfery. I. Okeana. **6**, 513–522 (1970).
27. A. Tonizzo, T. Harmel, A. Ibrahim, A. Gilerson, and S. Ahmed, "Estimation of the attenuation coefficient of the water body using polarimetric observations," Proc. SPIE **8030**, 803003 (2011).
28. A. Ibrahim, T. Harmel, A. Gilerson, A. Tonizzo, and S. Ahmed, "Exploring the relation between polarized light fields and physical-optical characteristics of the ocean for remote sensing applications," Proc. SPIE **8160**, 81600H (2011).
29. S. Maritorena, D. A. Siegel, and A. R. Peterson, "Optimization of a semianalytical ocean color model for global-scale applications," Appl. Opt. **41**(15), 2705–2714 (2002).
30. I. Ioannou, A. Gilerson, B. Gross, F. Moshary, and S. Ahmed, "Neural network approach to retrieve the inherent optical properties of the ocean from observations of MODIS," Appl. Opt. **50**(19), 3168–3186 (2011).
31. M. S. Twardowski, E. Boss, J. B. Macdonald, W. S. Pegau, A. H. Barnard, and J. R. V. Zaneveld, "A model for estimating bulk refractive index from the optical backscattering ratio and the implications for understanding particle composition in case I and case II waters," J. Geophys. Res-Oceans **106**(C7), 14129–14142 (2001).
32. A. Gilerson, A. Tonizzo, T. Harmel, A. Ibrahim, and S. Ahmed, "Polarization techniques for the retrieval of water parameters from above and below water polarimetric observations," Proc. SPIE **8372**, 83720T, (2012).
33. R. Spurr, K. Stamnes, H. Eide, W. Li, K. X. Zhang, and J. Stamnes, "Simultaneous retrieval of aerosols and ocean properties: A classic inverse modeling approach. I. Analytic Jacobians from the linearized CAO-DISORT model," J. Quant. Spectrosc. Ra. **104**(3), 428–449 (2007).
34. H. H. Tynes, G. W. Kattawar, E. P. Zege, I. L. Katsev, A. S. Prikhach, and L. I. Chaikovskaya, "Monte Carlo and multicomponent approximation methods for vector radiative transfer by use of effective Mueller matrix calculations," Appl. Opt. **40**(3), 400–412 (2001).
35. G. W. Kattawar, G. N. Plass, and S. J. Hitzfelder, "Multiple scattered radiation emerging from rayleigh and continental haze layers. 1: Radiance, polarization, and neutral points," Appl. Opt. **15**(3), 632–647 (1976).
36. H. C. Van de Hulst, *Light scattering by small particles* (Dover Publications, 1981).
37. A. Gilerson, J. Zhou, S. Hlaing, I. Ioannou, J. Schalles, B. Gross, F. Moshary, and S. Ahmed, "Fluorescence component in the reflectance spectra from coastal waters. Dependence on water composition," Opt. Express **15**(24), 15702–15721 (2007).

#174765 - $15.00 USD Received 21 Aug 2012; revised 16 Oct 2012; accepted 23 Oct 2012; published 29 Oct 2012

38. M. I. Mishchenko, L. D. Travis, and A. A. Lacis, *Scattering, absorption, and emission of light by small particles* (Cambridge University Press, 2002).
39. G. W. Kattawar, S. J. Hitzfeld, and J. Brinstock, "Explicit form of Mie phase matrix for multiple scattering calculations in I, Q, U and V representation," J. Atmos. Sci. **30**(2), 289–295 (1973).
40. A. M. Ciotti, M. R. Lewis, and J. J. Cullen, "Assessment of the relationships between dominant cell size in natural phytoplankton communities and the spectral shape of the absorption coefficient," Limnol. Oceanogr. **47**(2), 404–417 (2002).
41. Z. Lee, K. L. Carder, and R. A. Arnone, "Deriving inherent optical properties from water color: a multiband quasi-analytical algorithm for optically deep waters," Appl. Opt. **41**(27), 5755–5772 (2002).
42. R. M. Pope and E. S. Fry, "Absorption spectrum (380-700 nm) of pure water. II. Integrating cavity measurements," Appl. Opt. **36**(33), 8710–8723 (1997).
43. G. W. Kattawar and C. N. Adams, "Stokes vector calculations of the submarine light-field in an atmosphere-ocean with scattering according to a Rayleigh phase matrix - effect of interface refractive-index on radiance and polarization," Limnol. Oceanogr. **34**(8), 1453–1472 (1989).
44. C. D. Mobley, "Estimation of the remote-sensing reflectance from above-surface measurements," Appl. Opt. **38**(36), 7442–7455 (1999).
45. A. Tonizzo, T. Harmel, A. Ibrahim, S. Hlaing, I. Ioannou, A. Gilerson, J. Chowdhary, B. Gross, F. Moshary, and S. Ahmed, "Sensitivity of the above water polarized reflectance to the water composition," Proc. SPIE **7825**, 78250F (2010).
46. T. Harmel, A. Gilerson, S. Hlaing, A. Tonizzo, T. Legbandt, A. Weidemann, R. Arnone, and S. Ahmed, "Long Island Sound Coastal Observatory: assessment of above-water radiometric measurement uncertainties using collocated multi and hyperspectral systems," Appl. Opt. **50**(30), 5842–5860 (2011).
47. T. Harmel, A. Tonizzo, A. Ibrahim, A. Gilerson, J. Chowdhary, and S. Ahmed, "Measuring underwater polarization field from above-water hyperspectral instrumentation for water composition retrieval," Proc. SPIE **8175**, 817509 (2011).
48. S. Hlaing, A. Gilerson, T. Harmel, A. Tonizzo, A. Weidemann, R. Arnone, and S. Ahmed, "Assessment of a bidirectional reflectance distribution correction of above-water and satellite water-leaving radiance in coastal waters," Appl. Opt. **51**(2), 220–237 (2012).

1. Introduction

Light-scattering properties of particles in the ocean and atmosphere have been extensively studied. Taking note that solar radiation is initially completely unpolarized, once it reaches the Earth's atmosphere, scattering events, such as Rayleigh (molecular) and particulate scattering, cause it to become partially polarized [1]. In atmospheric sciences of the Earth and other planets, these effects are used in retrieval algorithms that take polarization into consideration. Although various ground, airborne and satellite sensors provide information about light scattered by the atmosphere-ocean system (AOS), only a few of them measure polarization characteristics of light. Light exhibits, as a result of scattering, some degree of polarization (DoP) in different directions, and this polarization is directly related to the source of the radiation and to the properties of the scatterers. Thus, the polarization state of light carries information about the AOS that can be utilized for remote sensing [2,3] of microphysical and optical properties of particulates including the oceanic hydrosols [4–7].

Increasing efforts are being made to explore the relation between polarization features of the underwater light field and the inherent optical properties (IOPs) of oceanic and coastal waters, such as absorption and attenuation coefficients of hydrosols suspended in the water body. Estimating the components of the Stokes vector of the polarized water-leaving radiance, emerging from the ocean, at the top of the atmosphere (TOA) is a challenging task for satellite applications. This is mainly because of the relatively small magnitude of the polarized water-leaving radiance and the large contribution of polarized light, mostly singly scattered, by atmospheric molecules and particulates. Nevertheless, it has been shown that the contribution of the Stokes components of the water-leaving radiance at the TOA is not negligible for blue light over open ocean waters [8,9] and for near-infrared light from bright coastal waters [5].

In the planetary atmosphere, polarized light is mainly singly scattered by molecules and aerosols, giving a polarization signature at the TOA that directly corresponds to the angular feature of the polarized phase function or Mueller matrix of the atmospheric particles [10]. Therefore, features primarily originating from single scattering can be readily identified in the angular distribution of the degree of linear polarization (DoLP) [10]. In the open ocean, the majority of particles are organic particles (both living and nonliving), whose concentrations

#174765 - $15.00 USD Received 21 Aug 2012; revised 16 Oct 2012; accepted 23 Oct 2012; published 29 Oct 2012

co-vary with chlorophyll concentration [Chl]. These types of particles induce a weak depolarizing effect on the underwater DoLP caused by molecular scattering, due to low relative refractive index [3]. Underwater polarization is, therefore, mainly driven by Rayleigh scattering by water molecules resulting in a relatively simple DoLP pattern [11–13]. On the other hand, in coastal waters, hydrosols are mainly composed of two types of particles: non-algal and algal. Algal particles with high water content have a low refractive index (approximately 1.06) relative to that of water and are therefore poor distinctive scatterers [13–15]. They can impact polarization fields only primarily through their absorption features. Non-algal particles (NAP), such as minerals, are more effective scatterers due to their high relative refractive index, typically around 1.18 [16]. These particles can significantly decrease the DoLP of the water-leaving radiance and should be more easily detectable than organic particles in the open ocean. Although the DoLP is highly sensitive to scattering [4,17], absorbing properties of the water also significantly impact the polarized light field: increase of absorption usually corresponds to the decrease of the number of the scattering events and leads to an increase of the DoLP. Thus, colored dissolved organic matter (CDOM), typically a strong absorber of light present in coastal waters, increases the DoLP [9].

Several approaches were proposed for the retrieval of water parameters from polarized observations [3,5,18–20] but have not been fully implemented yet for various technical reasons. For example, Chami et al. [18] suggest that it is possible to retrieve the suspended particulate matter (SPM) from the measurements of the DoLP at the Brewster angle using a derived empirical relationship. That relationship is limited to calm sea states and high inorganic concentrations. It was also suggested that the current polarimeteric satellites such as the POLarization and Directionality of the Earth's Reflectances (POLDER) instrument on Polarization and Anisotropy of Reflectances for Atmospheric Sciences coupled with Observations from a Lidar (PARASOL) [21] and the planned Multi-viewing, Multi-channel, and Multi-polarization Imager (3MI) instrument [22] having multi-directional and polarized measurements capability can be used for such retrievals. Regrettably, these sensors are mainly designed for aerosol retrieval studies and have very coarse spatial resolution (6-7 km). This makes the retrievals and their validation of useful ocean parameters very difficult, especially in coastal waters where the IOPs can rapidly change, even over short distances. Besides that, atmospheric correction is a very important aspect that needs to be taken into account for retrievals over coastal waters due to the increased heavy presence of aerosols over these regions and non-negligible water-leaving signal in the near-infrared part of the spectrum.

It was recently shown that DoLP patterns of underwater light are quite stable, even when the sea surface is ruffled by strong winds, and can be well predicted by vector radiative transfer (RT) simulations based on known IOPs [11,23–25]. Thus, a more accurate retrieval of oceanic parameters can be possible by the measurements of the polarized water- leaving radiance.

Remote sensing reflectance (R_{rs}) is defined as the water-leaving radiance normalized by the sum of direct and diffuse downwelling irradiances. It is, to a first approximation, proportional to b_b/a for open ocean waters and to $b_b/(a + b_b)$ for coastal waters, where b_b is the total backscattering coefficient and a is the total absorption coefficient. As such, R_{rs} by itself does not contain any information on the light forwardly scattered into the water. At the same time, studying polarized radiance scattered in milky solutions, Timofeyeva [26] found a relationship between the DoLP and "the parameter T which is equal to the ratio of the attenuation coefficient of the scattered light flux to the direct light flux". This parameter is in turn well connected to the attenuation/absorption ratio c/a, where c is equal to $a + b$ and b is the scattering coefficient, hence, $c/a = (a + b)/a = 1 + (b/a)$. Our recent studies [27,28] showed that at some viewing angles a relation between the DoLP and the attenuation/absorption ratio exists for waters with a very broad variability of constituents and thus can be used for the retrieval of c/a from the measured DoLP and retrieving c if a is known.

On the other hand, standard retrieval algorithms estimate the backscattering coefficient b_b, not the scattering coefficient b, and therefore assumptions on the backscattering ratio have to

#174765 - $15.00 USD Received 21 Aug 2012; revised 16 Oct 2012; accepted 23 Oct 2012; published 29 Oct 2012

be made to determine the scattering coefficient b [29,30]. The backscattering ratio varies between 0.5% (in open ocean) and 3% (in coastal waters with high mass concentrations of inorganic particles [31]). In coastal waters, the complexity of the water composition is higher, since interactions with shores and rivers discharge of sediments and nutrients lead to unpredictable variability of the type of water constituents and their relative concentrations. As a result, a new approach needs to be developed in order to avoid the rough estimate of the backscattering ratio, which leads to high inaccuracies in the retrievals of the scattering or attenuation coefficients.

The present article extends the initial study of Timofeyeva and our related work [27,28,32] focusing on the dependence of the DoLP on the IOPs for a broad range of bio-optical and microphysical parameters. DoLP measurements are especially advantageous because the DoLP is independent of the absolute calibration of related sensors [9,23,33].

The purpose of this study is to explore, in detail, the relation between DoLP and c/a for various water compositions and for particles with various microphysical properties. We primarily focus our attention on coastal waters, where the particles strongly affect the polarization of the upwelling light. The study is based on a theoretical analysis encompassing a large range of realistic parameters. First, the bio-optical and the radiative transfer models are described in Section 2. The results of the radiative transfer simulations and the analysis of the measurements of the DoLP for the retrieval of optical properties are then presented in Section 3 followed by the conclusions in Section 4.

2. Radiative transfer modeling

2.1. Theoretical background

The RayXP program [34] was used to simulate the transfer of radiation in homogenously scattering, plane parallel media. Generally, polarized radiation moves through the coupled system of atmospheric layers, through the surface of the ocean (air-water interface), and through the oceanic layers. Since the system is considered to be plane parallel, each layer is characterized by its own molecular and aerosol or hydrosol extinction coefficient (c), single scattering albedo (ω), and Mueller matrix ($\boldsymbol{F}$). The propagation of light into the medium is governed by the vector radiative transfer equation (VRTE),

$$\mu \frac{\partial \mathbf{S}(\tau, \mathbf{n})}{\partial \tau} = \frac{\omega(\tau)}{4\pi} \iint \mathbf{F}\left(\tau, \mathbf{n}, \mathbf{n}'\right) \mathbf{S}\left(\tau, \mathbf{n}'\right) d\mathbf{n}' - \mathbf{S}(\tau, \mathbf{n}), \tag{1}$$

where $\mathbf{S}(\tau,\mathbf{n})$ is the Stokes vector of the light in the direction $\mathbf{n}(\mu,\varphi)$; $\mu = \cos(\theta)$ and θ and φ are the zenith and azimuth angles in a spherical coordinate system; τ is the optical thickness of the medium and $\mathbf{F}$ is its scattering matrix.

The program optimizes computational time by incorporating various techniques, collectively called the Multicomponent Approach (MCA), for solving the VRTE. They include the multicomponent approximation, the Fourier expansion of the transfer equation, the small angle solution, and the adding doubling method. The MCA separates the scattering matrix of the scatterer into two main components. It separates the peaked component from the more diffused remaining component of the scattering matrix. Each of these two separate components are further divided into multiple components that are generally easy to solve for the VRT equations, significantly reducing the computational time without compromising the accuracy of the RT general solution [34]. The outputs of the vector radiative transfer code are the Stokes elements of underwater radiance (at a specific optical depth). The DoLP can then be calculated as

$$DoLP = \frac{\sqrt{Q^2 + U^2}}{I}, \tag{2}$$

#174765 - $15.00 USD Received 21 Aug 2012; revised 16 Oct 2012; accepted 23 Oct 2012; published 29 Oct 2012

where I is the total radiation, Q and U are the linearly polarized components of the Stokes vector representing linearly polarized radiance. The circularly polarized radiance, V, is assumed to be negligible [35].

2.2. Bio-optical model

In this work, we simulated the atmosphere-ocean system assuming two simple, plane-parallel, homogeneous layers. The first layer is dedicated to the atmosphere, assuming Rayleigh (molecular) scattering only. For simplification, no aerosols are included in this analysis. Rayleigh optical thickness values are taken from MODIS products (0.098 at 550 nm) and the molecular optical properties are obtained from the standard data bank provided with RayXP, with a molecular depolarization factor of 0.0279 [36]. No gas absorption is included in the modeled atmospheric layer. The second layer is dedicated to the ocean, which is assumed optically deep in order to minimize bottom boundary effects. A wind speed of 3 m/s, is assumed for the wind-ruffled surface between the atmosphere and the ocean.

The optical properties of the oceanic layer were generated using the bio-optical model detailed in Gilerson et al. [37] and references therein. We use a realistic and representative four component bio-optical model of typical coastal waters. The constituents included water itself, non-algal particulates (*i.e.* mineral), (NAP), chlorophyll-containing particles (phytoplankton) and CDOM. We use the subscripts 'w,' 'nap,' 'ph,' and 'g,' respectively, to identify these four components. We are limiting the maximal concentrations of NAP and [Chl] to be 10 g/m^3 and 20 mg/m^3, respectively and the maximal absorption of CDOM at 400 nm to 3 m^{-1}. Minimal concentrations of NAP and Chl are 0.5 g/m^3 and 1 mg/m^3, respectively and CDOM absorption is 0.3 m^{-1} which corresponds to relatively clear water conditions.

Specific absorption coefficients of phytoplankton and NAP and specific scattering coefficient for NAP particles were assumed to be constant at the reference wavelength in order to minimize the effects of the variability of the assumed model and to focus on the effects of varying particulate concentrations and related scattering matrices. In Fig. 1, the flow diagram explains the bio-optical and the RT modeling. The input parameters are the real part of the bulk refractive indices for phytoplankton particles and NAP (1.06 and 1.18 respectively). For simplification, it is also assumed that both types of particles are homogeneous spheres. The scattering matrices are calculated with the Lorenz-Mie theory for a Junge (or hyperbolic) particle size distribution (PSD) for a specific range of particles radii using a code developed by Mishchenko et al. [38]. The structure of such matrices is as follows:

$$\mathbf{F}(\theta_{\text{scat}}) = \begin{bmatrix} F_{11} & F_{12} & 0 & 0 \\ F_{12} & F_{22} & 0 & 0 \\ 0 & 0 & F_{33} & F_{34} \\ 0 & 0 & -F_{34} & F_{44} \end{bmatrix} \tag{3}$$

The first element of the scattering matrix $\mathbf{F}$, F_{11}, is the phase function, and the rest of the components are the elements of the scattering matrix computed for spherical particles, whose symmetry is responsible for the zeros [36,39]. Although that assumption may not be true for the type of particles that occupy the water body in coastal waters, it is an approximation good enough to simulate the DoLP in these water conditions [9]. The scattering matrix is a function of the scattering angle (θ_{scat}) which is the angle between the incident light and the scattered light. Although we assume fixed refractive indices for both types of particles, the calculated bulk scattering matrix is a mix that depends on the scattering coefficients of phytoplankton particles and NAPs (derived from the bio-optical model) as follows [36]:

$$\mathbf{F}_{\text{Bulk}} = \frac{b_{\text{nap}} \times \mathbf{F}_{\text{nap}} + b_{\text{ph}} \times \mathbf{F}_{\text{ph}}}{b_{\text{nap}} + b_{\text{ph}}}, \tag{4}$$

#174765 - $15.00 USD Received 21 Aug 2012; revised 16 Oct 2012; accepted 23 Oct 2012; published 29 Oct 2012

where $\mathbf{F}_{\text{Bulk}}$ is the bulk scattering matrix resultant from the mixing of the NAP scattering matrix ($\mathbf{F}_{\text{nap}}$) and the phytoplankton scattering matrix ($\mathbf{F}_{\text{ph}}$). The variability in the calculations of the bulk scattering matrix is directly dependent on the particulate concentrations in the bio-optical model. The radii of both phytoplankton particles and NAP were assumed between 0.1 and 50 μm with the slope (ξ) of the Junge-type particle size distribution (PSD) equals to 3.5, 4.0, and 4.5 for each type of particles. These three different slopes cover the typical range of different types of particles in the ocean [31]. By independently varying all the parameters, for the two particle types, we were able to cover a large range of IOPs typical of both open ocean and of coastal waters.

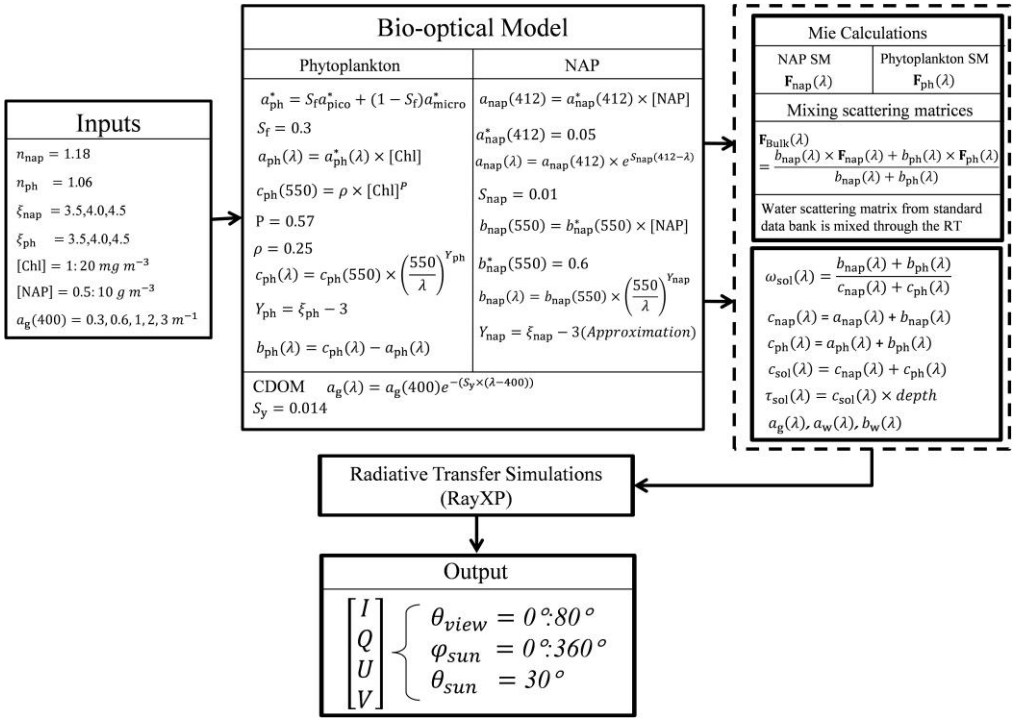

Fig. 1. Flow Diagram of the bio-optical and RT models for the generation of the data set.

In the block of the bio-optical model in Fig. 1, the specific absorption of the phytoplankton a^*_{ph}, which is spectrally dependent, is obtained using the model of Ciotti et al. [40] for the single size factor S_{f} = 0.3. The spectral attenuation coefficient of the phytoplankton $c_{\text{ph}}(\lambda)$ is a function of the exponent Y_{ph}, which is directly related to the slope of the hyperbolic particle size distribution shown in the input block [31]. The scattering coefficient $b_{\text{ph}}(\lambda)$ is calculated as the difference between the attenuation and the absorption coefficients. The absorption coefficient of the non-algal particles $a_{\text{nap}}(\lambda)$ is modeled as an exponential decaying function [16], where $a_{\text{nap}}(412)$ is the product of the NAP concentration and specific NAP absorption a^*_{nap} at 412 nm, which is fixed at 0.05 m^2/g. Similarly, the NAP scattering coefficient b_{nap} at the reference wavelength of 550 nm, is the product of NAP concentration and specific scattering b^*_{nap} at 550 nm, which is fixed at 0.6 m^2/g. The spectral NAP scattering coefficient $b_{\text{nap}}(\lambda)$ is also modeled as a power law function with the power directly related to the particle size distribution. CDOM absorption coefficient $a_{\text{g}}(\lambda)$ is calculated as an exponentially decaying function with a fixed slope S_{y} of 0.014 according to Babin et al. [15].

The bio-optical model for the simulation of the spectral IOPs described above uses three main parameters as inputs: the concentration of chlorophyll, [Chl], the concentration of non-algal particles, [NAP], and the CDOM absorption coefficient at 400 nm, $a_{\text{g}}(400)$. We use a

#174765 - $15.00 USD Received 21 Aug 2012; revised 16 Oct 2012; accepted 23 Oct 2012; published 29 Oct 2012

logarithmic distribution [30] to describe the variability of particulate concentrations in water. There are 15 different cases for both [Chl] and [NAP] and 5 cases for $a_g(400)$. Since the number of cases for each type of particulate concentrations is limited to 15, the distribution of the input does not have a great effect on the output results.

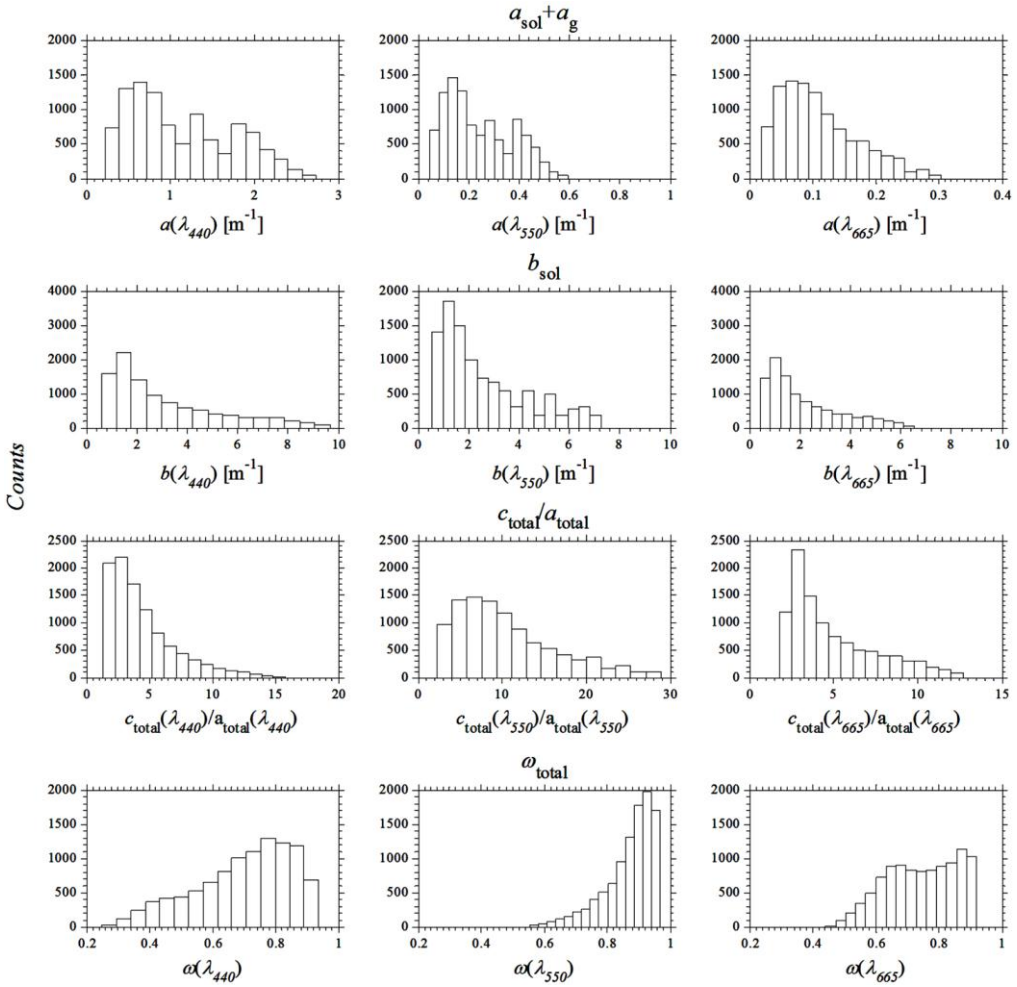

Fig. 2. Histogram of hydrosol plus CDOM absorption coefficients 'a_{sol} + a_g', hydrosol scattering coefficients 'b_{sol}', total attenuation to absorption ratio 'c_{total}/a_{total}', and total single scattering albedo 'ω_{total}', at 440, 550, and 665 nm wavelengths.

To generate the RayXP data sets, the different [Chl], [NAP], $a_g(400)$, PSDs of each type of particles were permutated into 10125 different cases. For each one of these cases, four main parameters were needed for RayXP: the spectral attenuation, the single scattering albedo, the bulk scattering matrix, and the CDOM absorption. Figure 2 shows the histograms of the hydrosols absorption coefficient (a_{sol}) plus CDOM absorption coefficient (a_g) and scattering coefficient (b_{sol}) with the subscript '*sol*' for particles (phytoplankton particles and NAP), CDOM absorption with the subscript 'g'; absorption and attenuation with subscript 'total' for hydrosol plus CDOM plus water, and single scattering albedo (ω_{total}) at three chosen wavelength (440, 550, and 665 nm).

In Fig. 2, we obtained simulations for a broad range of water conditions including highly scattering waters, often found in coastal areas. The single scattering albedo, ω_{total}, which is the ratio of NAP and phytoplankton plus water scattering coefficients to their attenuation coefficients plus CDOM absorption coefficient, is a representative of optical properties in

#174765 - $15.00 USD Received 21 Aug 2012; revised 16 Oct 2012; accepted 23 Oct 2012; published 29 Oct 2012

oceans. As can be seen from Fig. 3, a greater weight is placed on the scattering properties of NAP in the calculation of the bulk scattering matrices from Eq. (4). The bulk (or mixed) scattering matrix matches more closely the shape of the NAP scattering matrix since the scattering coefficient of NAPs are much higher than the scattering coefficient of phytoplankton particles. Figure 3 shows the phase function and the normalized polarization components of the Mie scattering elements (F_{11}, F_{12}/F_{11}, F_{33}/F_{11}, and F_{34}/F_{11}) for one case of chlorophyll and NAP concentrations and slope of PSD, as an illustration. The polarization elements (F_{12}/F_{11}, F_{33}/F_{11}, and F_{34}/F_{11}) of the scattering matrix of phytoplankton particles follow the shape of pure Rayleigh scattering since the relative refractive index is very low, *i.e.* 1.06. The matrix is calculated for spherical shaped particles. On the other hand, the shape of the polarized scattering matrix elements of NAPs looks different due to their high refractive index except for the near forward and backward direction where it exhibits a weak polarization effect according to the Mie-Lorenz theory.

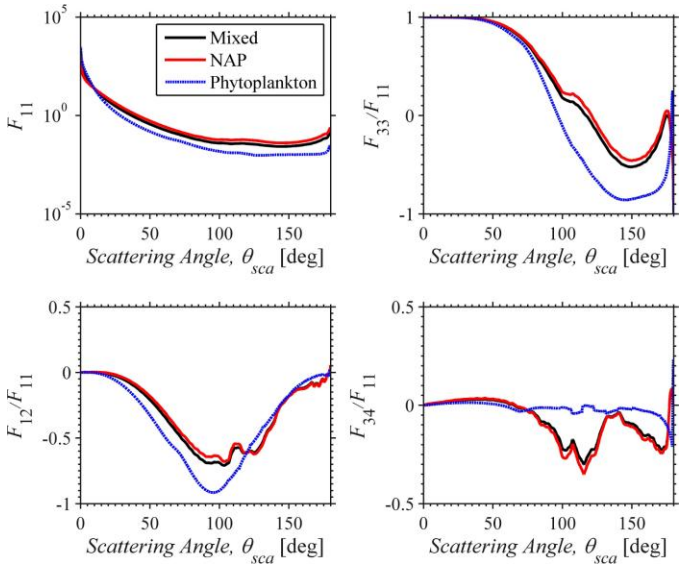

Fig. 3. Phase function and normalized polarization elements of the scattering matrix from Mie calculations for one case as an illustration for n_{nap} = 1.18, n_{ph} = 1.06, ξ_{nap} = 4.0, ξ_{ph} = 4.0, [NAP] = 1.45 g m^{-3}, and [Chl] = 10.5 mg m^{-3} at 440 nm.

3. Results and discussion

3.1. Parameterization of the relationship

In this section, simulated radiative transfer outputs of DoLP are investigated in order to find a definitive relationship with the IOPs, in terms of the attenuation to absorption ratio (c/a). Such a relationship would give us the possibility of retrieving the attenuation coefficient, c, of the water constituents from data obtained by under- or above-water polarization radiometer measurements of the upwelling radiation, since the absorption coefficient, a, is routinely estimated from the remote sensing reflectance using well-established algorithms [30,41].

The results presented below were obtained from simulations at three wavelengths (440, 550, and 665 nm) at depths just below the air-water interface. Regarding the sun angle and the viewing geometry, we fix a single solar zenith angle (*i.e.* 30°) and vary the viewing angle to cover the largest range of scattering angles in the backward direction. The range which corresponds to the aperture of Snell's window, whose border is shown by dashed lines in Fig. 4 is the one in which we are mostly interested because of the possibility of future above-water remote sensing measurements of the DoLP. In Fig. 4, we show the angular plot of the DoLP for three relative azimuth angles equal to 0°, 40°, and 90° at the three aforementioned

#174765 - $15.00 USD Received 21 Aug 2012; revised 16 Oct 2012; accepted 23 Oct 2012; published 29 Oct 2012

wavelengths. The plot shows the dependence of the DoLP on the *c*/*a* ratio by the color gradation from light to darker grey or black. Light grey corresponds to values of the DoLP calculated for low *c*/*a* ratio, whereas dark grey represents high *c*/*a* ratios. In another sense, this color gradation could also corresponds to the single scattering albedo, where higher *c*/*a* ratio means less absorption, more scattering, and higher single scattering albedo in the medium, therefore producing lower DoLP. Similarly for lower *c*/*a* ratio, it means less scattering and lower single scattering albedo producing higher DoLP.

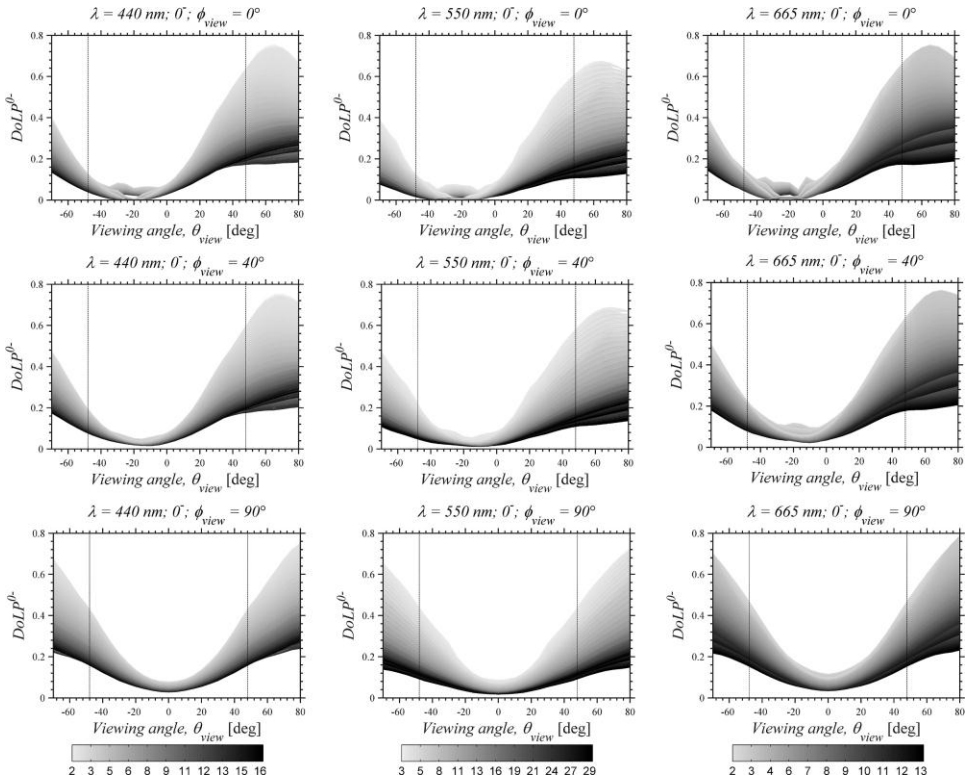

Fig. 4. DoLP just below water surface vs. viewing angle between –70° and 80° (0° for vertically downward), sun zenith 30° and relative azimuth plane 0°, 40°, and 90° at three wavelengths (440, 550, and 665 nm). The grey color gradation corresponds to varying values of *c*/*a*. Lighter grey is for lower *c*/*a* ratio, while darker is for higher *c*/*a* ratio. The dashed vertical lines correspond to the angles of the borders of Snell's window.

We can also notice that the color gradation is not linear, especially in the 440 and 550 nm due to the logarithmic distribution assumed for constituents' concentrations ([Chl] and [NAP]) and therefore absorption and scattering coefficients. On the other hand, the DoLP at 665 nm shows a less noticeable variability of color gradation since the optically dominant component is water absorption which is assumed to be constant [42].

The scattered plots in Fig. 5, 6, and 7 represent the variability of the DoLP just below the surface, $DoLP^{0-}$, at different viewing and azimuth angles (0° for nadir viewing angle and 180° for zenith; by convention the azimuth angle is equal to 0° when the Sun and the sensor are in opposition) versus *c*/*a* ratio at 440, 550, and 665 nm. Each of the three different colors corresponds to a different slope of the PSD. We focus only on the slope of the NAP particles because of their dominant weight on the calculation of the bulk phase matrix and on the DoLP accordingly simulated.

#174765 - $15.00 USD Received 21 Aug 2012; revised 16 Oct 2012; accepted 23 Oct 2012; published 29 Oct 2012

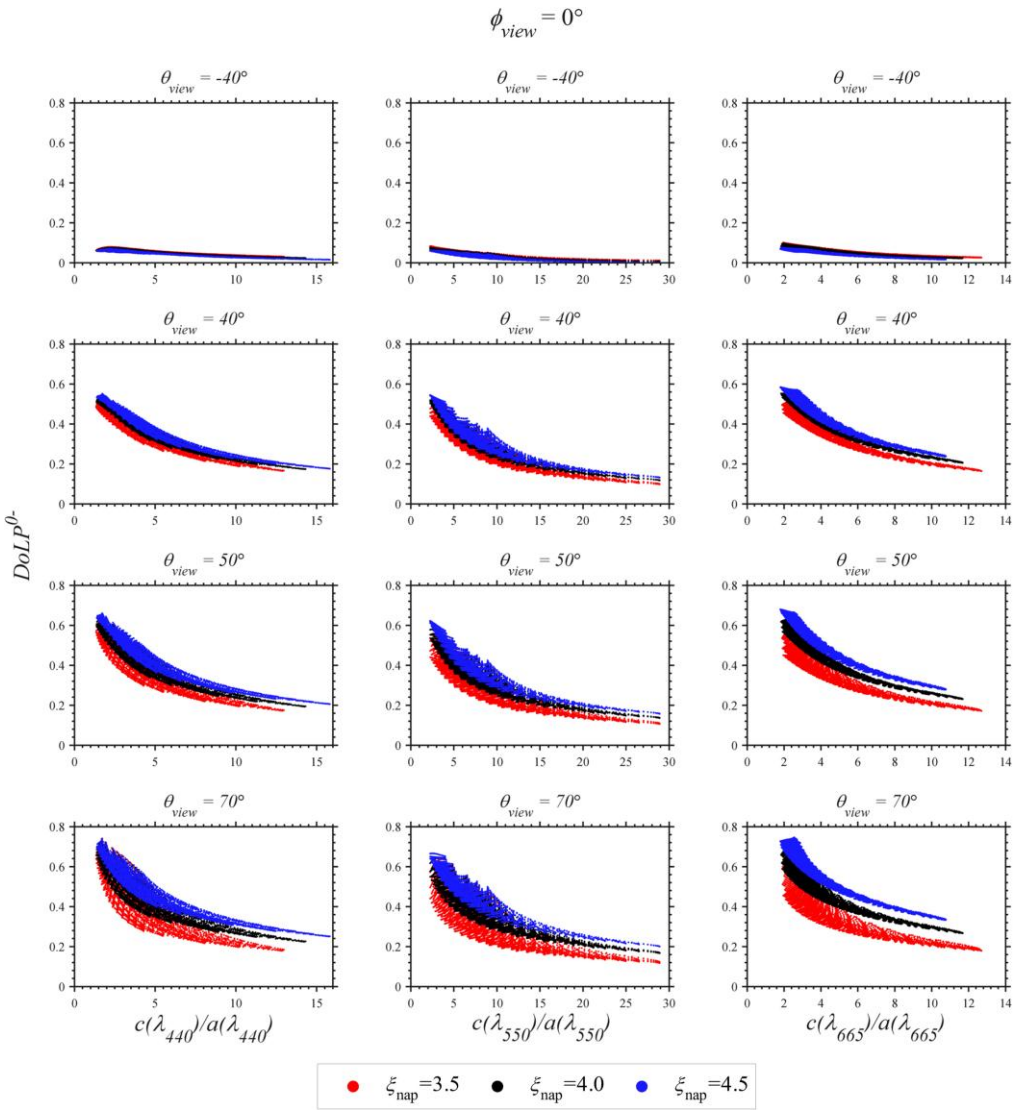

Fig. 5. The relation between DoLP and *c*/*a* at three wavelengths at different viewing angles and for sun relative azimuth of 0° for three slopes of the NAP PSD, *i.e*. 3.5, 4.0, and 4.5. Sun zenith angle is fixed at 30°.

It can be noticed that the relationship between DoLP and *c*/*a* ratio dramatically degrades in the viewing geometry (*i.e*. θ_{view} = –40°) that corresponds to a large (*i.e*. close to 180°) scattering angle where the DoLP is least sensitive due to the nature of scattering of light according to Mie theory. These angles are between –40° to 0°, where the negative sign shows that the observer is in the anti-solar plane where the sun is behind the sensor for the assumed sun zenith of 30°. Between the viewing angles 0° and 20°, the relationship exhibits a shape similar to the shape corresponding to other viewing angles, for example, 40°, but with smaller variability since these angles are far from the maximal DoLP. The maximum of DoLP typically falls between 90° and 110° scattering angle [11], depending on the type of constituents present in the water body, which corresponds to nearly 70° viewing angle for our sun geometry; however, these viewing angles are outside Snell's window. High sensitivity of the DoLP versus the *c*/*a* ratio is obvious in Fig. 5, 6, and 7. The sensitivity of the DoLP to the

#174765 - $15.00 USD Received 21 Aug 2012; revised 16 Oct 2012; accepted 23 Oct 2012; published 29 Oct 2012

slope of the PSD of NAPs is slightly higher at the wavelength of 665 nm when compared to 440 and 550 nm.

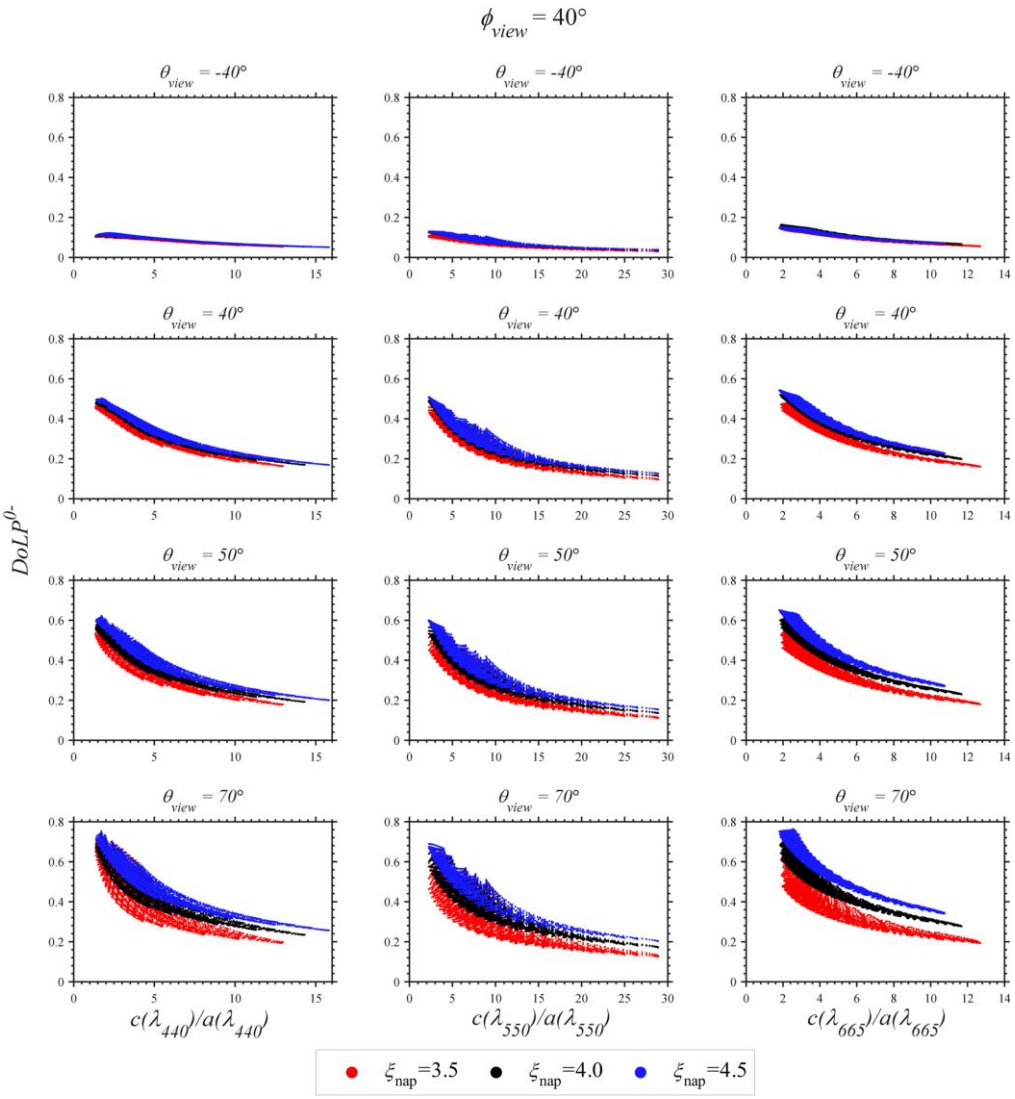

Fig. 6. The relation between DoLP and *c*/*a* at three wavelengths at different viewing angles and for sun relative azimuth of 40° for three slopes of the NAP PSD, *i.e.* 3.5, 4.0, and 4.5. Sun zenith angle is fixed at 30°.

The Fig. 5, 6, and 7 show a strong relationship between the DoLP and *c*/*a* ratio with high variability in the broad range of both parameters for specific viewing angles (20°-50°) in the sun's main plane, and at 40° and 90° away from it (this range of viewing angles in water corresponds to 27°-82° viewing angles in the air). As a result, it is possible to easily fit the relationship, which allows us to retrieve the attenuation coefficient given the DoLP measurements and the absorption coefficient (which can be retrieved with good accuracy using inversion algorithms [30]) plus a prior knowledge of the slope (ξ) of the PSD of NAPs.

#174765 - $15.00 USD Received 21 Aug 2012; revised 16 Oct 2012; accepted 23 Oct 2012; published 29 Oct 2012

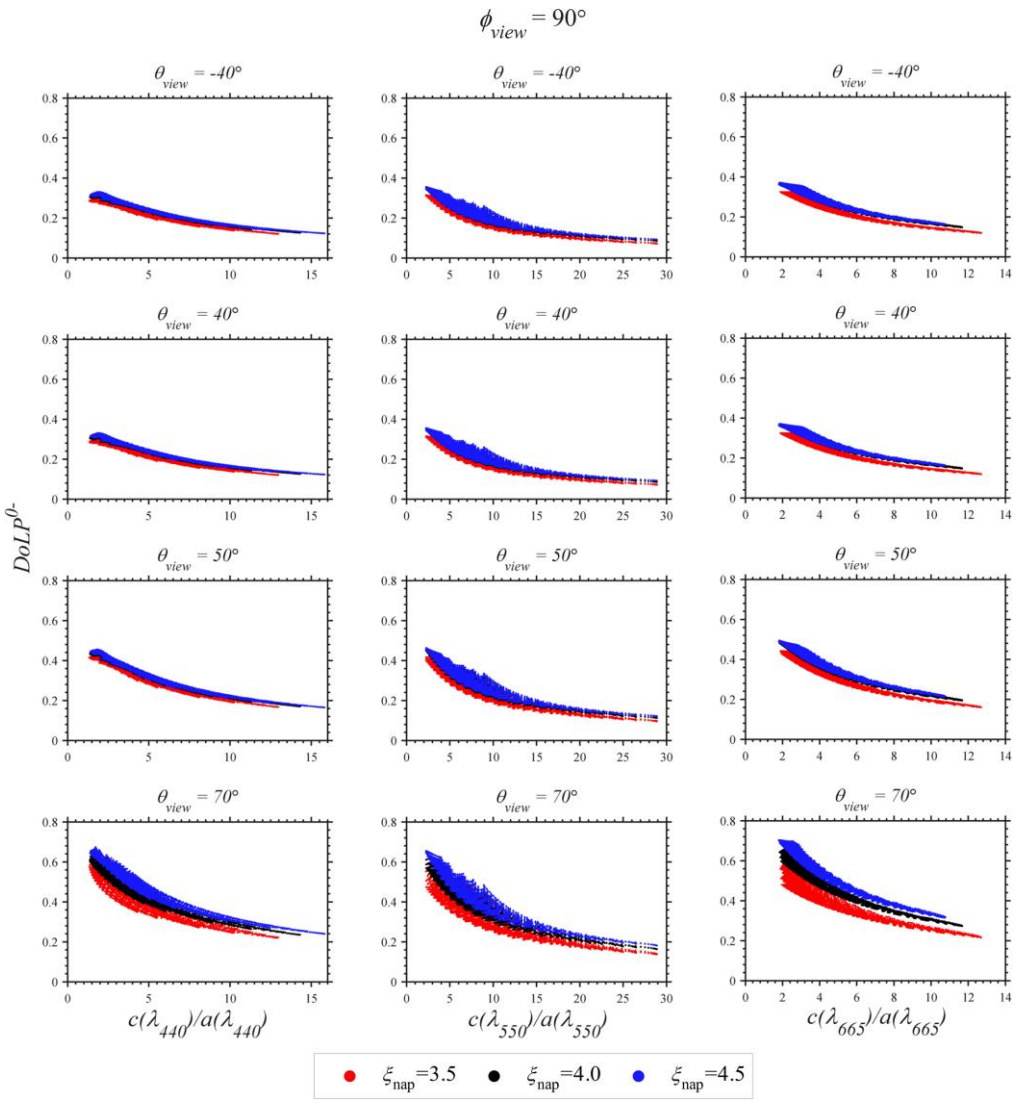

Fig. 7. The relation between DoLP and *c*/*a* at three wavelengths at different viewing angles and for sun relative azimuth of 90° for three slopes of the NAP PSD, *i.e.* 3.5, 4.0, and 4.5. Sun zenith angle is fixed at 30°.

The parameterized relationship was estimated using a power law fitting for the three PSD slopes of NAPs as follows:

$$\left\{\left(\frac{c}{a}\right)_{\text{fit}}\right\}_{\xi_{\text{nap}}=3.5,4.0,4.5} = \left\{\chi(DoLP)^{\gamma}\right\}_{\xi_{\text{nap}}=3.5,4.0,4.5}, \quad (5)$$

where a and c are the absorption and attenuation coefficients, respectively; χ and γ are the fitting coefficients. The power law fitting is believed to be a good method because of its simplicity in representing the bio-optical properties of the water (c/a) using only two parameters; this also agrees with the results shown by Timofeyeva [26]. Although we used a fourth order polynomial for the fitting in our previous work [28,32], the power law fitting showed residuals similar to the polynomial fittings.

#174765 - $15.00 USD Received 21 Aug 2012; revised 16 Oct 2012; accepted 23 Oct 2012; published 29 Oct 2012

In Fig. 8, the relationship between the IOPs (c/a ratio) and the DoLP is parameterized as a power law as in Eq. (5) with a good coefficient of determination R^2 (squared correlation) opening the possibility for an accurate retrieval technique of the attenuation coefficient. While deriving a final semi-analytical or analytical relationship between DoLP and c/a are not the main goals of this paper, nevertheless it is important to show that a relationship exists between the polarization signature of the ocean and its bio-optical, microphysical, and geo-chemical properties. An interesting result shown in Fig. 8 is that the fits for both ξ_{nap} of 4.0 and 4.5 are similar for the all three wavelengths. In coastal waters, the slope ξ_{nap} of PSD of NAP largely falls in the range 4.0-4.5, where these particles are small in size [14,31]. Since the relationship weakly depends on the PSD of chlorophyllic particles, a rough estimate of ξ_{nap} to be in its typical range may not induce large errors in, for example, retrieval analysis.

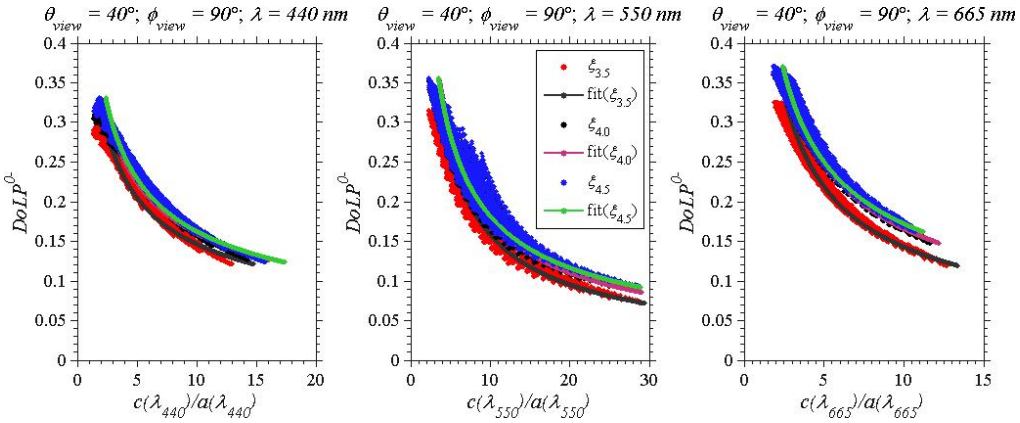

Fig. 8. Fitted relationship between DoLP at θ_{view} = 40° and φ_{view} = 90° and c/a ratio at three wavelengths for three different NAP slopes of the particle size distribution (PSD).

The quality of the fitting of Eq. (5) can be estimated by calculating the root mean squared error (RMSE) or the coefficient R^2 between the parameterized/fitted values and the resultant values of the radiative transfer simulations. A high correlation or a low RMSE value indicates a good quality of the fitting and vice-versa. The coefficient of determination is calculated as follows:

$$R^2 = \frac{SSR}{SST} = \frac{\sum_{i=1}^{10125}\left[\left(\frac{c}{a}(DoLP_i)\right)_{fit} - \overline{\left(\frac{c}{a}\right)_{fit}}\right]^2}{\sum_{i=1}^{10125}\left[\left(\left(\frac{c}{a}\right)_i\right) - \overline{\left(\frac{c}{a}\right)_{fit}}\right]^2}, \quad (6)$$

where SSR is the sum of squared differences between the regression predictions or fit ($(c/a(DoLP_i)_{fit}$) and the sample mean of (c/a) with the over bar in Eq. (6), where 'i' iterates from 1 to 10125 different cases of IOPs in the RT simulations. The SST term stands for sum of squares total which means the sum of squared deviations of the (c/a) values around their mean.

In order to have a synoptic view of the fitting quality, the R^2 values are plotted in Fig. 9 for all the viewing geometries available for a given solar angle (*i.e.* θ_{sun} = 30°). In this manner, we can estimate the range of geometries that permits one to obtain the best accuracy for the retrieval of the attenuation (and the scattering, $b = c-a$) coefficient based on measurements of the DoLP. Similar results were found from RMSE distributions.

#174765 - $15.00 USD Received 21 Aug 2012; revised 16 Oct 2012; accepted 23 Oct 2012; published 29 Oct 2012

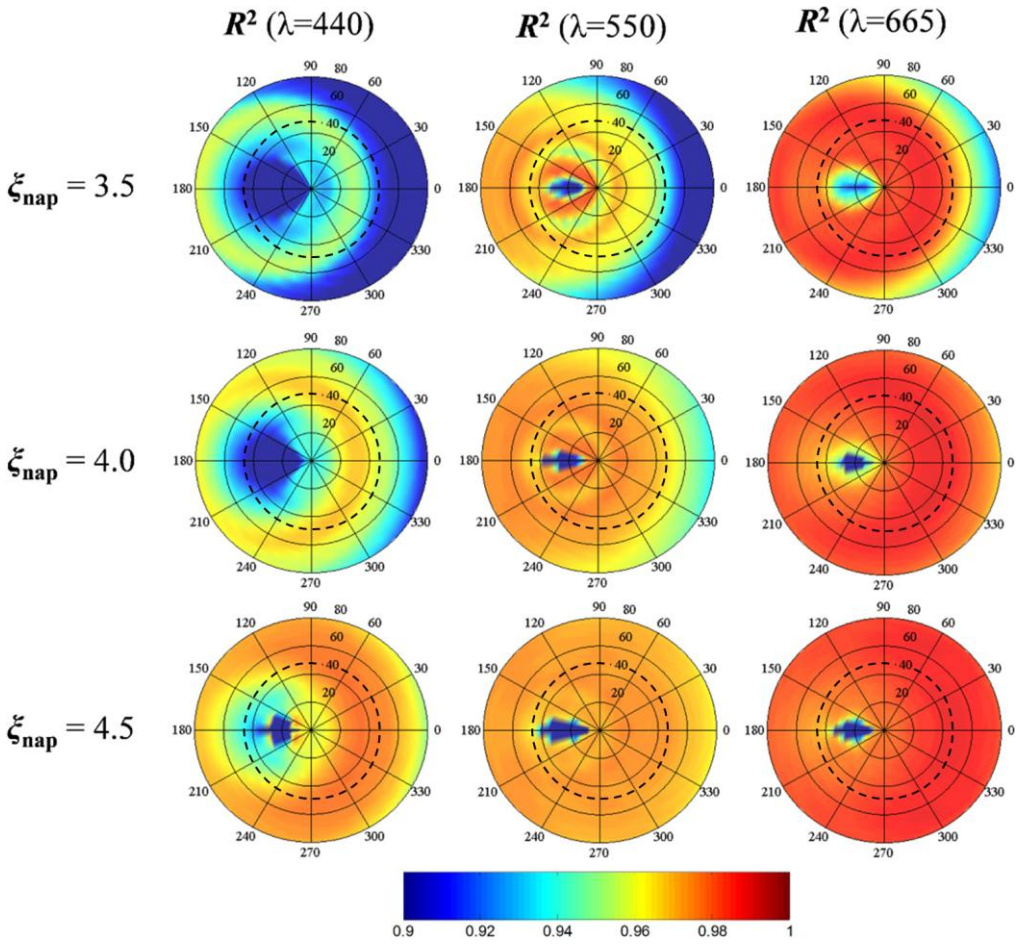

Fig. 9. Synoptic view of the coefficient of determination R^2 at just below the air-water interface for sun relative azimuth from 0° to 360° (0° azimuth is for sun and sensor are in opposition) and viewing angle of upwelling polarized light from 0° to 80° (0° viewing angle is for sensor looking vertically downward). Dashed lines correspond to the borders of Snell's window.

In Fig. 9, the coefficient of determination (R^2) for most of the viewing geometries below the water surface is higher than 0.9. That indicates a good and consistent relationship between the simulated data set and the fitting obtained using the power law function in Eq. (5). It is also noticeable that R^2 degrades in the backscattering direction where the DoLP is theoretically minimal (DoLP ~ = 0). That region is in the anti-solar plane (180° relative azimuth, between 150° and 210°) and between viewing angles ranging from 0° to just slightly higher than 40° for ξ_{nap} of 3.5 and 4.0 at 440 nm and between 0° to 20° for ξ_{nap} of 3.5, 4.0 and 4.5 at 550 and 665 nm. Less steep slopes of NAP PSD are not typical in the ocean; they correspond to higher density of large NAP, which can have a highly depolarizing effect on the upwelling radiance. As a result, degradation in the relationship between DoLP and c/a is probably due to the decrease in the sensitivity of the DoLP. It can be seen from Fig. 9 that waters with larger-sized NAP (ξ_{nap} of 3.5) exhibit lower R^2 compared to other slopes of NAP PSD.

The high (squared) correlation in Fig. 9 is very promising when considering future air- or space-borne measurements of the polarized water-leaving radiance, since it does not limit the range of viewing angles at which this type of sensors operate. For example, the good correlation that exists at the meridian plane away (90° away, for instance) from the sun's main plane (and therefore away from sun glint contaminations), makes the measurements of

#174765 - $15.00 USD Received 21 Aug 2012; revised 16 Oct 2012; accepted 23 Oct 2012; published 29 Oct 2012

polarized water-leaving radiance easier and more accurate and opens the possibility of a direct estimation of the attenuation coefficient, otherwise physically impossible, using above water sensors. It is obvious from Fig. 9 that the best R^2 values can be achieved at 665 nm for a broad range of azimuth and viewing angles. This is most likely due to the moderate absorption (usually dominated by the water absorption) which reduces the number of the scattering events and increases DoLP in comparison with 550 nm case. Details of these effects should be further studied.

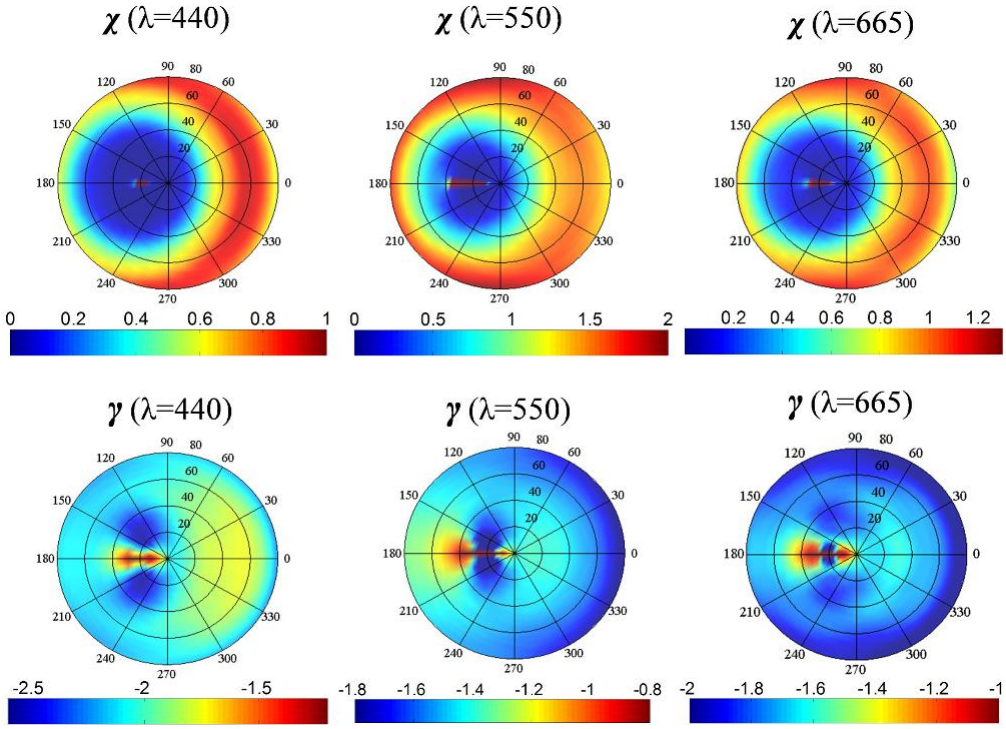

Fig. 10. Synoptic view of the fitting coefficients χ and γ at three wavelengths and ξ_{nap} = 4.0 at just below the air-water interface for sun relative azimuth from 0° to 360° (0° azimuth is for sun and sensor are in opposition) and viewing angle of upwelling polarized light from 0° to 80° (0° viewing angle is for sensor looking vertically downward).

Figure 10 gives a synoptic view of the fitting coefficients for the power law function in Eq. (5). It is noticeable that the fitting coefficients depend on the wavelength as well as the viewing geometry for this scenario where the sun position is fixed. These fitting coefficients should explain the variability between DoLP and *c*/*a* ratio.

3.2. Assessment of the relationship for above water detection

A feasible remote sensing algorithm requires a comprehensive analysis of the relationship between the bio-optical variables and the optical characteristics of light above the water surface. It was shown in the previous section that a strong relationship exists between DoLP and *c*/*a* for various viewing geometry at just below the air-water interface. In this Section the relationship is analyzed for conditions above the interface and is carried out by transmitting the Stokes components using the transmission matrix given in Kattawar et al. [43] for a flat sea-surface. Only the underwater upwelling light within Snell's window would be transmitted to above water, since the light outside the 96° cone suffers a total internal reflection due to the interface. Since the sun zenith angle in our simulations is assumed to be 30°, the maximal DoLP typically falls at scattering/viewing angles outside Snell's window. As a result, the maximal range of DoLP is undetectable from above water measurements. A further analysis has been done in order to propose a set of viewing geometries optimal for above-water

#174765 - $15.00 USD Received 21 Aug 2012; revised 16 Oct 2012; accepted 23 Oct 2012; published 29 Oct 2012

detection. In Fig. 11, a synoptic view of the coefficient of determination R^2 is calculated to assess the relationship between the DoLP and the *c*/*a* ratio for three PSDs, three wavelengths and all geometries at just above the water surface.

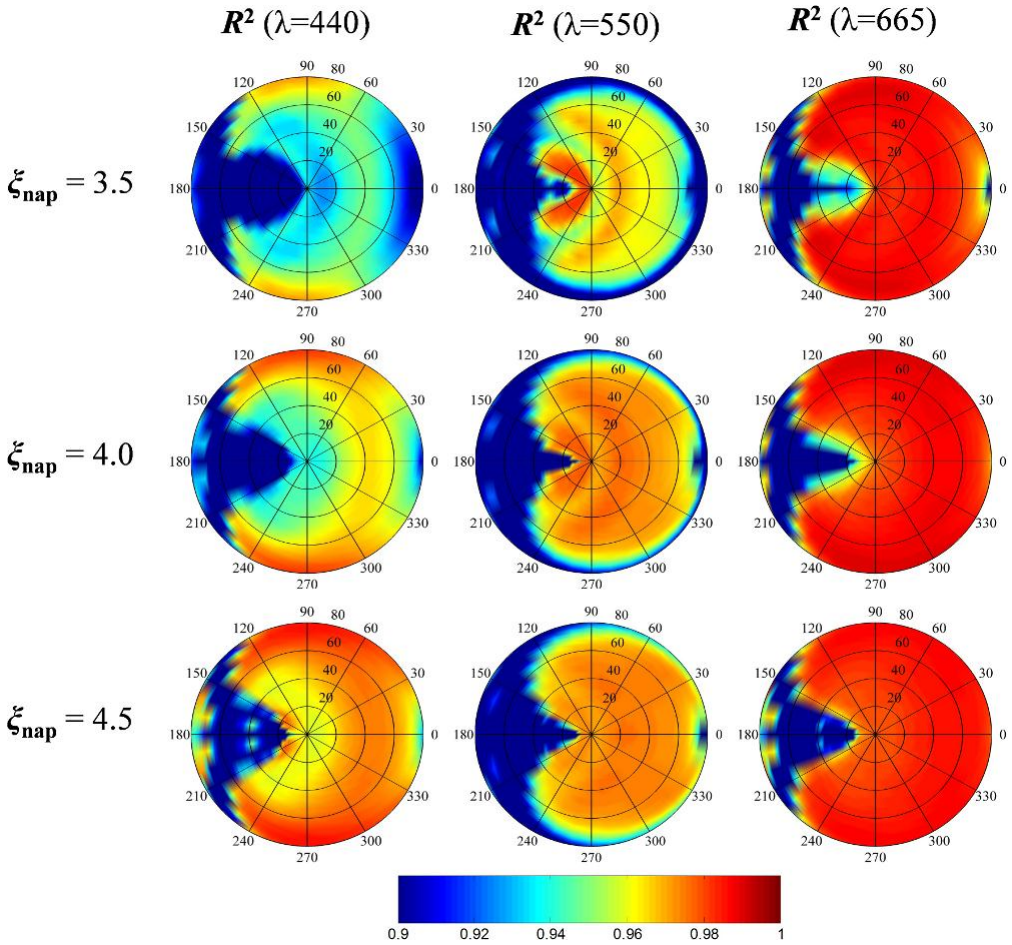

Fig. 11. Synoptic view of the coefficient of determination R^2 at just above the air-water interface for sun relative azimuth from 0° to 360° (0° azimuth is for sun and sensor are in opposition) and viewing angle of upwelling polarized light from 0° to 80° (0° viewing angle is for sensor looking vertically downward).

In Fig. 11, as expected, the R^2 values significantly deteriorate in the backscattering direction. The low correlation region which was clearly noticeable below water expands to a larger range of angles above the water due to light refraction. The transmission of the DoLP to above-water results in a lower correlation than below-water, generally degrading the variability of the DoLP versus *c*/*a* relationship. On the other hand, Fig. 11 shows a large range of viewing geometries with R^2 values higher than 0.9 in the main solar plane and away from it. For above water observations it is important to acquire measurements that are not contaminated by the sun glint which is maximal in the main plane. Sun glint reflection can be avoided by performing measurements at azimuth angles between 90° and 135° [44] with respect to the sun. Unfortunately, the DoLP of water-leaving radiance is typically highest in the sun's main plane and at large viewing angles near the borders of Snell's window. As a result, high values of DoLP tend to occur at higher viewing angles near the horizon. These limitations of the DoLP and R^2 values intersect, suggesting ideal viewing zenith angles between 40° and 60°, and a relative viewing azimuth angle of 90° as a preliminary estimation.

#174765 - $15.00 USD Received 21 Aug 2012; revised 16 Oct 2012; accepted 23 Oct 2012; published 29 Oct 2012

It can be seen that the limitations are much smaller for the 665 nm wavelengths where high R^2 values are observed for a broad range of viewing conditions as in the case for the below air-water interface conditions.

Further analysis needs to be performed also to take into account varying sun positions. The sun zenith is a major factor that can change both the magnitude of DoLP and R^2 values versus the geometry. For example, when the sun is near the horizon (large zenith), the maximal values of DoLP shift towards the inside of Snell's window and can be detected above water. Small sun zenith angle or overhead sun leads to highly depolarized upwelling radiance for most of the viewing geometries and therefore undetectable polarization signal. In Fig. 12 we show the DoLP of water-leaving radiance ($DoLP^{0+}$) versus the sun zenith angle from 0° to 70° for four cases of water conditions ranging from clear oceanic waters to turbid coastal waters, while we fixed ξ for both types of particles to 4.0, and for fixed CDOM absorption coefficient a_g at 400 nm to 0.6, with 60° viewing and 90° azimuth angles to ensure a detectable polarized signal above-water.

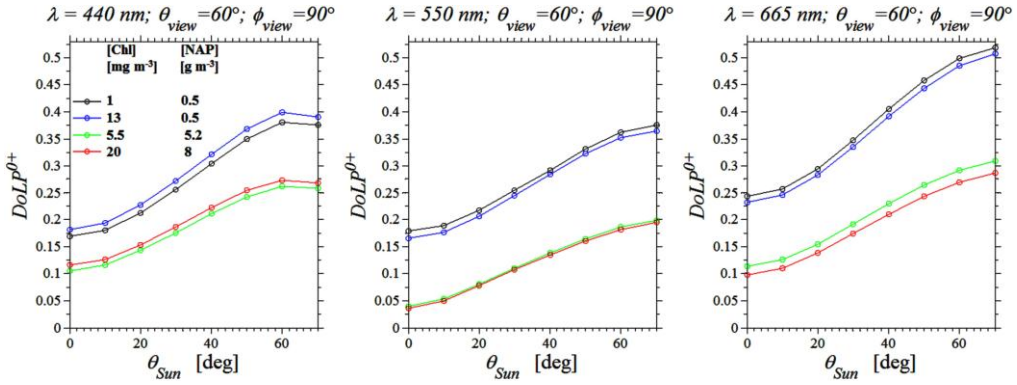

Fig. 12. DoLP versus the sun zenith angle θ_{Sun} = 0°-70° for θ_{view} = 60°, φ_{view} = 90° at 440, 550, and 665 nm.

The DoLP in Fig. 12 is seen to be sensitive to three variables; primarily sun angle, water condition, and wavelength at which the signal was simulated. As expected, the DoLP increases with higher sun zenith angle. So the preferable sun angle should be around 50° at which point the reflectance signal will also remain high.

The dependence of the DoLP on the water conditions is noticeable. The signals from the water with high [Chl] and low [NAP] (blue curve) and low [NAP], low [Chl] (black curve) are highly polarized for all wavelengths, whereas higher turbidity (*i.e.* high [NAP]) leads to smaller detectable polarized signal above the water (red and green curve). The DoLP for low [NAP] cases (black and blue curves) show a significant increase from 440 to 665 nm, while more turbid cases (green and red curves) show just a small increase in DoLP for all sun angles. In all cases, concentrations of chlorophyllic particles do not have a significant effect on the DoLP. At green wavelengths, the total absorption coefficient is smaller than at blue and red wavelengths. This leads to the decrease of DoLP for high [NAP] cases (green and red curves). In conclusion, it is obvious that the DoLP is highly sensitive to the variability of water conditions for different wavelengths above the water and at optimal geometries. The sun position has a major impact on the magnitude of observed DoLP, whereas it does not have a profound effect on DoLP trends as a function of viewing angle for different water conditions, thus reducing ambiguity. Despite all the previously mentioned challenges, it is still possible and reasonable to move in the direction of retrieving bio-optical properties using above-water polarization measurements.

For future studies, in order to use the fitting coefficients of the power law function (in the form of look-up tables, for example) to estimate the attenuation coefficient, it is important to account for broader variability of bio-optical parameters, including the specific absorption and scattering coefficients of particulates, a^*_{ph}, a^*_{nap}, and b^*_{nap}, the size factor of

#174765 - $15.00 USD Received 21 Aug 2012; revised 16 Oct 2012; accepted 23 Oct 2012; published 29 Oct 2012

phytoplankton specific absorption S_f, and the slopes of the absorption and the scattering coefficients of the three main constituents of the ocean waters S_{nap}, S_y, Y_{ph}, and Y_{nap} . More importantly, in order to have a robust algorithm for retrievals, the DoLP versus c/a relationship should be comprehensively tested above the water surface and for specific viewing geometries, using either satellite, air-borne, or sensors on fixed observational platform and for varying sun position. This approach can be readily applied to under- or above-water measurements, such as those collected by the Long Island Sound Coastal Observatory (LISCO), in operation since October 2009 [45–48], where the HyperSAS hyperpspectral instrument, equipped with two additional polarization sensitive water-leaving radiometers, is installed. Further simulations for above-water conditions will open the doors for more variables that affect the relationship mentioned in this study, including parameters of aerosols, wind speed and its effect on the ocean's surface, which all can significantly change the polarimetric signal at the TOA.

4. Conclusions

While attenuation and scattering coefficients are not retrievable from the scalar reflectance measurements, a relationship between the degree of linear polarization (DoLP) and the attenuation to absorption coefficients ratio (c/a) has been investigated using vector radiative transfer simulations for a large range of viewing geometries, wavelengths, and bio-optical and microphysical parameters typical of ocean and coastal waters for conditions just below the air-water interface. We showed that it is possible to fit, using a power law function, the relationship between the DoLP and the c/a ratio with a satisfactory coefficient of determination R^2 and with a relatively weak dependency on the particle size distribution. These results open a possibility for the retrieval of the attenuation and, further, the scattering coefficients of the water medium from the DoLP measurements assuming given absorption coefficient, which is routinely retrieved from remote sensing reflectance data. The relationship was also tested for above the air-water interface and showed high R^2 values for a broad range of viewing angles. Dependence of the relationship on the sun zenith angle was analyzed as well. The best viewing geometries for below water polarization measurements call for a viewing angle between 20° and 40° from the nadir direction, which is within the borders of Snell's window, and a relative azimuth of 90° with respect to the sun and for above the water viewing angles from 40° to 60° with relative azimuth of 90°. Established relationships can be tested in the future for many of the illumination and viewing conditions considered here, together with varying water properties at the LISCO site. Applications to above water polarization measurements, such as those provided by the LISCO instrumentation set are one of the main potential follow-ons of this work and of future validation studies.

Acknowledgments

We would like to thank the anonymous reviewer for the insightful reviews and remarks. We are also grateful to Dr. Eleonora Zege for scientific and technical support with the RayXP code. This work is partially supported by grants from NOAA and the Office of Naval Research.

#174765 - $15.00 USD Received 21 Aug 2012; revised 16 Oct 2012; accepted 23 Oct 2012; published 29 Oct 2012